Available online at www.sciencedirect.com
SCIENCE DIRECT®
Journal of Power Sources 135 (2004) 215–231
JOURNAL OF POWER SOURCES
www.elsevier.com/locate/jpowsour

From colloidal to composite electrolytes: properties, peculiarities, and possibilities

Binod Kumar*

University of Dayton Research Institute, Dayton, OH 45469-0170, USA

Received 30 January 2004; accepted 27 February 2004

Available online 24 June 2004

Abstract

This paper discusses the effects of a colloidal phase on the ionic conductivity and transport mechanism in liquid and polymer electrolytes. The conductivity enhancement due to the addition of diverse ceramic colloids is attributed to the formation and existence of double layers. These colloids and associated double layers also lead to time-dependent conductivity variation in a certain temperature range. Annealing and physical aging effects on conductivity originate from the existence and displacement of the double layer surrounding each colloidal particle. It has also been suggested that one can design and develop electrolytes for specific applications by selecting three critical elements: a conducting ion, a transport medium, and a network of double layers in a colloidal or composite electrolyte.

Keywords: Colloidal phase; Composites; Conductivity

1. Introduction

Electrolytes are of profound interest to chemists and engineers because of their application in electrochemical devices such as fuel cells, batteries, sensors, and displays. Presently, liquid electrolytes are the mainstay of many electrochemical devices; however, a need exists for solid electrolytes as substitutes for liquid electrolytes employed in the state-of-the-art electrochemical devices. The solid electrolytes provide many advantages over the liquid electrolytes such as ease of containment, thermal and chemical stabilities, and nonflammability. The colloidal and composite systems have the potential to develop tailored solid electrolytes with improved performance to cover a wider range of device application temperatures.

In a recent paper, Kumar and Rodrigues [1] reported electrochemical properties of colloidal electrolytes that are inherently liquid electrolytes in which nanosize ceramic particles are uniformly suspended. The presence of colloids in the liquid electrolytes creates a charged double layer of colloid–liquid interfacial regions which are believed to be associated with low migration energy of conducting ions. The conductivity and temperature dependence of these colloidal electrolytes are attractive for potential applications. Above the melting point, T_m, these colloidal electrolytes perform like a liquid electrolyte, whereas below the T_m they exhibit attributes characteristic of high conductivity composite electrolytes. The transition from colloidal to a solid composite phase and the associated effect on conductivity are intriguing features discussed in this paper. To our knowledge, this has not been reported in prior literature.

A considerable number of investigations on the ionic conductivity of composite materials have been conducted in the last three decades, and these investigations report major enhancements in the electrical conductivity of an ionically conducting matrix doped with an inert particle phase. Four review papers within the last 5 years [2–5] document the developmental history and general characteristics of these fast ionic composite conductors.

This paper culminated from our work on liquid, polymer, and polymer–ceramic composite electrolytes over the last 10 years. Various segments of this paper have already been independently published and their themes will be included and cited appropriately in the text. The purpose of this paper is to present a comprehensive view of the characteristics and potentials of electrolytes developed from colloidal/composite systems. It is also recognized that this endeavor crosses boundaries among various disciplines of science and therefore attempts will be made to use fundamental principles to explain and account for the experimental observations ob-

* Tel.: +1-937-229-3527; fax: +1-937-229-3433.
E-mail address: kumar@udri.udayton.edu (B. Kumar).

0378-7753/$ – see front matter © 2004 Elsevier B.V. All rights reserved.
doi:10.1016/j.jpowsour.2004.04.038

tained from complex compositions of materials employed in the colloidal/composite electrolyte systems.

2. Experimental

Colloidal electrolytes were prepared by employing organic liquid electrolytes and nanosize ceramic powders. The liquid electrolytes were comprised of 1:1 solvent blend of ethylene carbonate (EC) and propylene carbonate (PC) with a molar concentration of lithium hexafluorophosphate ($LiPF_6$) and prepared in a dry box using dried solvents and salts. The colloidal electrolytes were formulated by mixing the liquid electrolytes with dried nanosize ceramic phase ($BaTiO_3$). The average particle size of $BaTiO_3$ was 1 μm.

The PEO:$LiBF_4$–ceramic (MgO, TiO_2, Al_2O_3, etc.) composite electrolyte films were prepared by the solvent and melt-casting techniques using high molecular weight (2,000,000) reagent grade poly(ethylene) oxide (PEO), lithium salts ($LiBF_4$, $LiPF_6$, etc.) and a nanosize ceramic phase. For the solvent-casting process, a solution of PEO (Union Carbide, molecular weight 2,000,000) and lithium salt in AR grade acetonitrile (Aldrich) was prepared in which the nanosize ceramic phase was dispersed and sonicated. After sonication, a homogenized colloidal solution was obtained which was cast and dried into a film form of about 100 μm thickness. The melt-casting process involved mixing the three components (PEO, lithium salt, and nanosize ceramic phase) in solid particulate forms, melting at about 175 °C for 15 min, and homogenizing with an electrically driven impeller. The process yielded a bulk preform that was subsequently used to make thin films (≃150 μm thick) using a film-maker. The melt-casting and film-making operations were conducted in a dry box. The properties of the composite electrolytes remained identical whether they were made by either solvent-casting or melt-casting. The processing time was reduced by a factor of 6 (24 h versus 4 h) in the case of melt casting, without the use of solvent. Therefore, it was a preferred technique and employed in the later stages of our 10 years of investigations.

The conductivity of liquid and colloidal electrolytes was measured using a two electrode cell with a cell constant of 0.46 cm. The electrodes were prepared from stainless steel with a surface area of 0.44 cm^2. The electrodes and electrolytes were contained in a glass tube which was sealed in a dry box. Subsequently, ac measurements were conducted to obtain complex impedance plots (z' versus z''). The conductivity was computed using the real part of impedance (z') and the cell constant (0.46 cm).

For the ac impedance measurements of the freestanding composite electrolyte films, a cell in the blocking electrode configuration (stainless steel (ss)/composite electrolyte/ss) was assembled using a special fixture. The ac impedance measurement was carried out using an EG&G (Model 398) and Solartron (Model 1290 with electrochemical interface) in the frequency range of 0.1 Hz–100 kHz. The cells were contained in a dry atmosphere glass vessel which was held in an environmental chamber that allowed a temperature dependence measurement in the −40 to 100 °C range. The set temperature was maintained within ±1 °C.

3. Results and discussion

3.1. Properties of colloidal systems and transport mechanisms

3.1.1. Space charge/double layer formation

After a nanosize ceramic particle such as silica (SiO_2) or alumina (Al_2O_3) is introduced in a liquid electrolyte, the electric charge and field associated with the particle interacts with the structure of the liquid electrolyte leading to the formation of a double layer or space charge. The interaction is schematically depicted in Fig. 1. A 10 nm diameter silica particle may have about 12,500 SiO_2 molecules. If there are only 12 electrons on the surface of the 10 nm particle, the electronic charge density would be 0.02 electrons/nm^3. This charge density is much lower than the ionic charge density; for example, O^{2-} has a charge density of 2000 electrons/nm^3. Thus, the electronic charge densities differ by approximately five orders of magnitude between the nanosize ceramic phase and ionic species. The constitution of a double layer as depicted in Fig. 1 may include free electrons at the surface of the nanosize ceramic phase, whereas cations and dipoles at the adjacent double layer balance the surface electronic charge. The dipoles may be the structural constituents of the liquid or a polymer phase in a given electrolyte system.

In a colloidal system the double layer can be formed or destroyed. A well-defined double layer provides stability in the system. The double layers associated with the ceramic particles will repel each other because they possess charges of the same sign. The collision of spherical colloids resulting from the Brownian motion may also lead to coalescence and precipitation of the ceramic particles which characterizes an unstable colloidal system.

The potential energy as a function of distance, r, between the spherical double layers in a colloidal system is depicted in Fig. 2. The total potential energy is comprised of two contributions: (a) the double layer interaction determined by the Gouy–Chapman potential ($\Psi_0 e^{-kr}$) and (b) the electrostatic repulsion ($-Ar^{-6} + Br^{-12}$) where k, A, and B are constants. From Fig. 2 it is noted that the electrostatic repulsion predominates at smaller values of r. The net energy, U_{Total}, is always positive, suggesting that the spherical double layer cannot stick together. The particles of colloidal dimensions do not aggregate to form microscopic dimensions because their boundaries are protected by electrified interfaces. The coulombic repulsion is fundamental to the stability of colloids and the potential energy is minimized and remains positive for stable colloidal electrolytes.

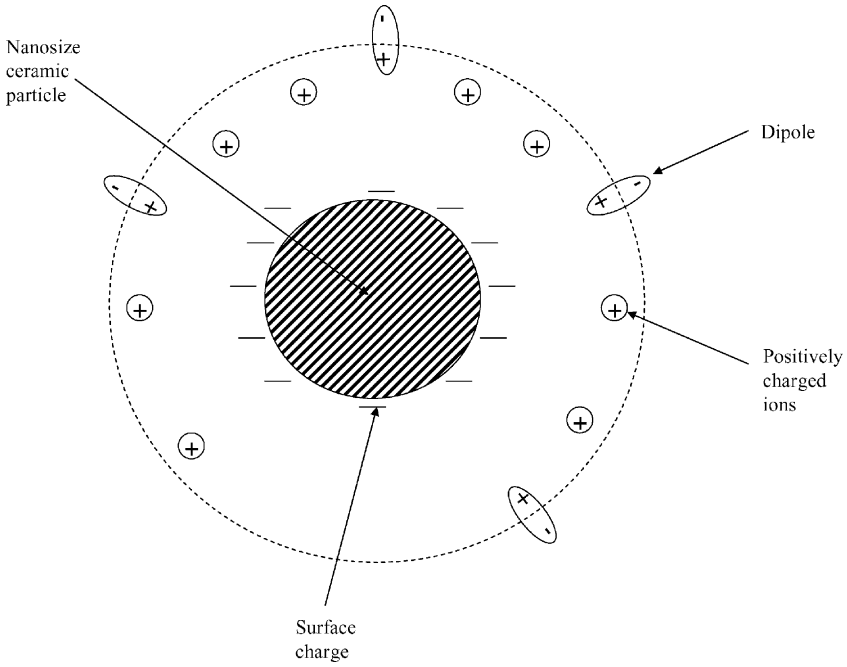

Fig. 1. Schematic presentation of the double layer/space charge formation around a nanosize ceramic particle.

If the colloidal spheres were not wrapped by electrified layers, interaction between the particles will dominate, as shown by the bottom curve of Fig. 2 and will have a minimum in negative potential energy, favoring aggregation of colloidal particles. The stability of the colloidal solution is primarily determined by controlling the concentration of the colloidal phase, in effect controlling the *r* parameter and thus the potential energy. Further discussion on this topic can be found elsewhere [6].

The formation and stability of a double layer is also temperature dependent. At higher temperatures, a diffuse double layer is expected because thermal energy (*kT*) will perturb dipole orientation and energy states of electrons. As the temperature is lowered towards absolute zero, the thermal energy induced motion of dipoles and electronic transition will diminish and consequently a sharply defined double layer will result. The thickness of the double layer may also be influenced because of the temperature variation.

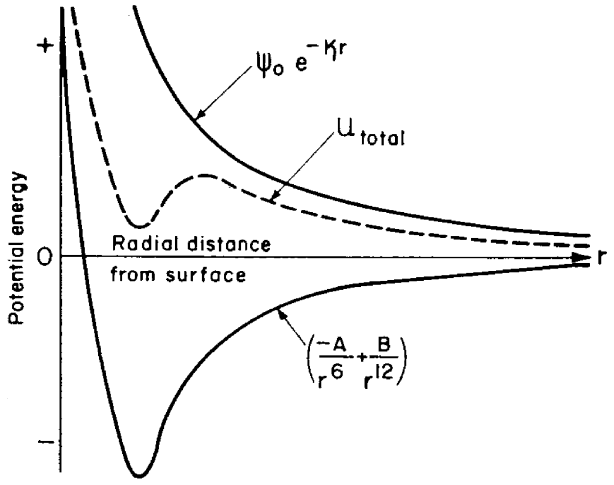

Fig. 2. The energy of interaction between two colloidal particles as a function of their distance apart, when the conditions favor stability of the colloid.

At higher temperatures, acidic or basic surface groups attached to the colloidal particles may not make any contribution to the formation of a double layer because of the Brownian motion and time averaging effect of the field associated with these colloidal surface groups. However, at lower temperatures the contribution of surface groups may become significant in the formation of a double layer as the degree of the time-averaged electric field is diminished.

3.1.2. Transition of a colloidal structure to a composite solid

The transition from a colloidal structure exhibiting a liquid-like behavior to a composite solid may take place through two different mechanisms. The first mechanism involves freezing the liquid-like structure into a rigid solid in which spatial positions of each colloid and the associated double layer are frozen. The second mechanism stems from the sol–gel type of transition in which there is a three-dimensional network of colloidal particles which are in close contact. The noncolloidal space is filled by the liquid phase. The first transition (liquid → solid) is characterized by a complete absence of liquid phase below the transition temperature, whereas the second transition (sol–gel) is associated with the presence of a liquid phase coexisting with a three-dimensional network of solid colloidal particles. Furthermore, the two transitions may be

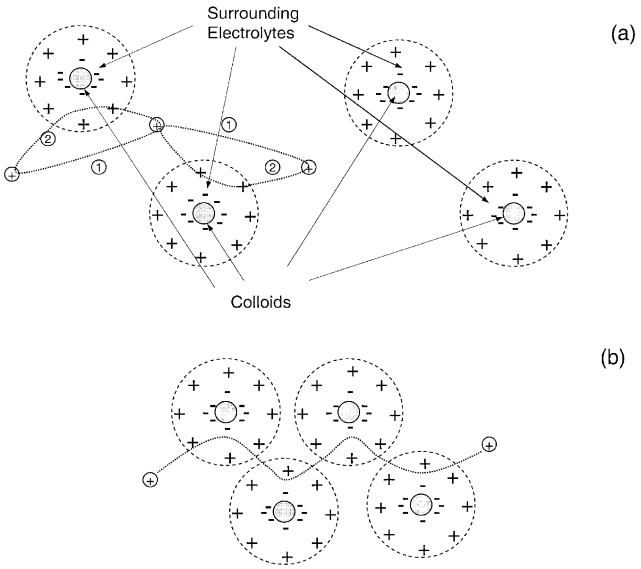

Fig. 3. (a) Colloidal electrolyte at higher temperatures ($>T_m$); (b) colloidal/composite electrolyte at low temperature ($<T_m$).

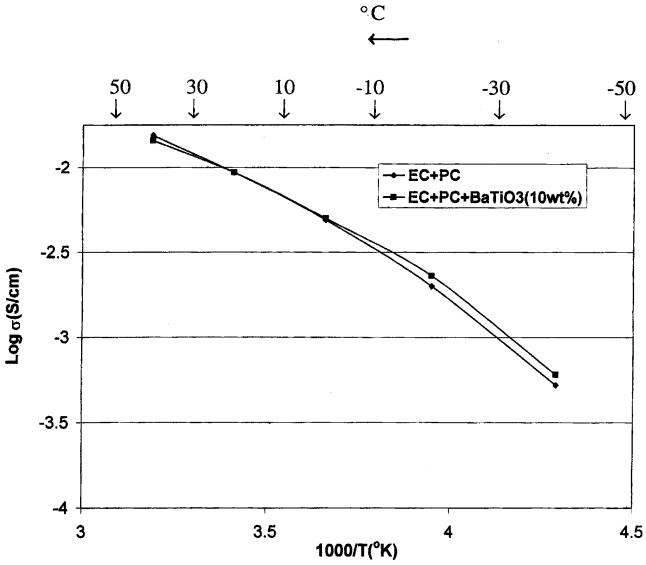

Fig. 4. Conductivity of a liquid electrolyte and a colloidal electrolyte containing 10 wt.% $BaTiO_3$.

differentiated by a characteristic double layer structure and associated properties. This paper is primarily concerned with the transition associated with the first mechanism.

3.1.3. Transport of charged species in colloidal systems

The space charge regions in colloidal systems are localized sources of electric fields. It is logical to expect that the movement of charged species will be influenced by these localized fields. The schematic views of transport paths of a conducting specie are illustrated in Fig. 3. If the colloidal system exhibits liquid-like properties, a positively charged specie may either be transported through the liquid phase (path 1) or through the double layer (path 2). Path 1 is more favorable because of the structurally assisted motion of conductive specie and its coordinating sphere. The structural assistance arises from a low viscosity, convective type of motion in the liquid state. This proposed mechanism will be substantiated with the experimental data in later sections of this paper. As the temperature is lowered, spherical double layers come in close proximity and the liquid phase may transition to a solid phase. Such a situation is schematically illustrated in Fig. 3(b). Now the transport of the charged species will take place through the double layer as it is energetically more favorable than the transport through the narrow, highly viscous liquid or solid phase.

3.2. Conductivity of colloidal electrolytes

An exploratory investigation on the role of a colloidal phase on the conductivity of a liquid, organic, lithium-ion conducting electrolyte has recently been reported [1]. This section will present a brief account of an interesting feature of these colloidal electrolytes. A liquid electrolyte comprising a 1:1 solvent blend of ethylene carbonate (EC) and propylene carbon (PC) with a molar concentration of lithium hexafluorophosphate ($LiPF_6$) exhibits a typical conductivity of liquids and is illustrated in Fig. 4. After mixing the liquid electrolyte with 1 μm dried barium titanate ($BaTiO_3$) powder with a concentration of 10 wt.%, the temperature dependence of conductivity was altered as presented in Fig. 4. The two conductivity curves of Fig. 4 intersect at about 20 °C. Above 20 °C, the $BaTiO_3$ containing electrolyte exhibits lower conductivities as compared to the liquid electrolyte. However, at temperatures below 20 °C, the colloidal electrolyte displays superior conductivities. The concentration of colloidal phase influences conductivities. At lower concentrations of $BaTiO_3$ powder the conductivity data are barely distinguishable as reported earlier [1].

After a microscopic particle of $BaTiO_3$ is introduced in the liquid electrolyte, the electric field associated with the surface charge of the particle interacts with the structure of the liquid electrolyte, leading to the formation of space charge regions. The interaction is temperature dependent and enhanced at lower temperatures. The volume of the liquid electrolyte, which is influenced by the microscopic $BaTiO_3$, is associated with high conductivity. As the concentration of the $BaTiO_3$ colloids increases, a larger volume fraction of the higher conductivity space charge regions is created. These eventually overlap and provide a three-dimensional network. The volume fraction of the colloidal phase must exceed the threshold to provide continuity of the high conductivity phase to reach a peak value of conductivity. The location of crossover points in the conductivity curves of liquid and colloidal electrolytes is related to the concentration of the colloidal phase [1].

The conductivity data of colloidal electrolytes presented in Fig. 4 appears to suggest that at higher temperatures, a liquid-like transport mechanism is the dominant contributor

to the conductivity. As the temperature is lowered, the viscosity of the colloidal electrolyte increases, the structural assistance to the transport of conducting specie decreases, and the liquid-like transport mechanism becomes weaker and the conduction pathways created through the space charge regions takes over.

3.3. Conductivity of polymer–ceramic composite electrolytes

Because of its popularity, poly(ethylene oxide) has been a polymer of choice for many studies; however, the choice of ceramic phase in the polymer–ceramic composite systems has been arbitrary and diverse. It may be argued that an ionic conducting matrix should facilitate the transport of lithium ions, which narrows the choice of the polymer component. But, what criteria should be used in selecting a ceramic component? This question was addressed by the author in an earlier publication [7]. In general, the ceramic components of composite electrolytes can be classified into two categories: active and passive. The active components are comprised of materials such as Li_3N and $LiAlO_2$. Due to the presence of lithium ions, these materials participate in the conduction process. The passive components are comprised of materials such as Al_2O_3, SiO_2, etc., which do not participate in the process. The choice between active and passive components has been quite arbitrary and perhaps needs further investigation, as these active and passive ceramic components would influence formation and structure of a double layer differently.

This section will present some experimental data on polymer–ceramic composite electrolytes employing passive ceramic components such as MgO, TiO_2, ZrO_2, and Al_2O_3.

3.3.1. PEO:$LiBF_4$–MgO system

This system was investigated and reported earlier [8] but selected experimental data will be presented to highlight important observations, as they augment a broader picture. Magnesium oxide (MgO) is a low density (3.58 gm cm^{-3}) ceramic with a positive free energy of reaction with lithium metal [7]. The free energy of reaction suggests that lithium passivation is unlikely to occur at the Li–MgO interface. Thus, this system is of commercial interest. The average particle size of MgO for the investigation was 15 nm.

3.3.1.1. PEO:$LiBF_4$ (8:1)–MgO (10 wt.%) electrolyte. Conductivity data of composite electrolyte films obtained from PEO:$LiBF_4$ (8:1)–MgO (10 wt.%) material are shown in Fig. 5. The specimen was heated to and stabilized at 100 °C for 30 min, cooled down to 20 °C, and held at that temperature overnight. Subsequently, it was again heated to and stabilized at 100 °C for 30 min before the conductivity measurements began. The conductivity data at each temperature was obtained after stabilizing the specimen for 30 min. After the temperature reached 20 °C, the specimen was allowed to remain at the temperature overnight. It is noted in Fig. 5 that $\log\sigma$ increased from −5.09 to −4.65. This conductivity enhancement resulting from isothermal stabilization is typical of composite electrolytes containing a ceramic phase, and the phenomenon will be explained later in this paper. As the temperature was lowered to −40 °C, the conductivity decreased monotonically. Again, the specimen was held overnight at −40 °C before the conductivity was measured during the heating cycle. The conductivities during the heating cycle are higher than conductivities registered during the cooling cycle. The conductivity data shown in Fig. 5 are comparable to the data reported by Croce et al. [9] on the PEO–$LiClO_4$, 10 wt.% TiO_2 electrolyte.

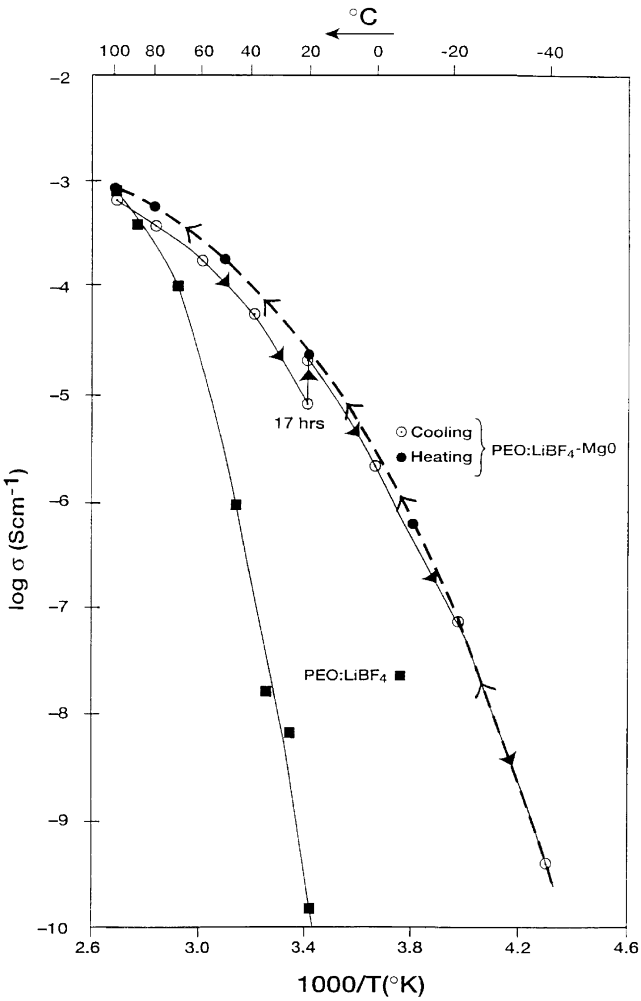

Fig. 5. Temperature dependence of conductivity of PEO:$LiBF_4$ (8:1)–MgO (10 wt.%) during heating and cooling cycles.

Also shown in Fig. 5 is the conductivity data of the PEO:$LiBF_4$ (8:1) polymer complex for comparison. The conductivity of the complex drops precipitously below 60 °C; at 20 °C this specimen has about four orders of magnitude lower conductivity than that of the composite electrolyte. The comparison clearly points out the role of MgO in retarding PEO crystallization and interacting with the polymer matrix, thereby imparting a beneficial effect on conductivity.

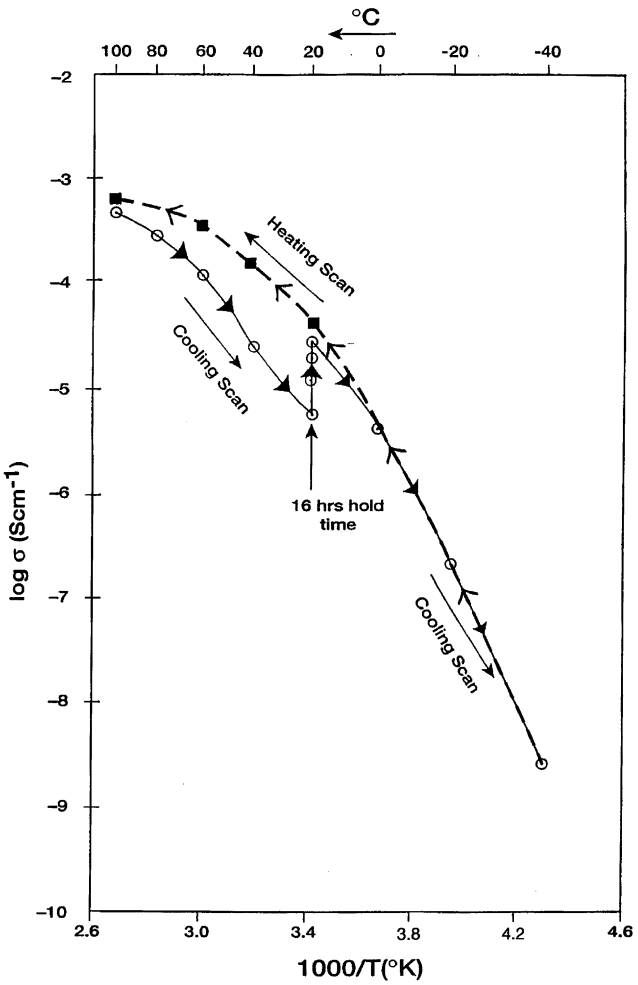

Fig. 6. Temperature dependence of conductivity of PEO:$LiBF_4$ (8:1)–MgO (20 wt.%) during heating and cooling cycles.

3.3.1.2. PEO:$LiBF_4$ (8:1)–MgO (20 wt.%) electrolyte. Conductivity data were obtained after cycling this specimen twice between 0 and 100 °C with a cumulative hold time of 18 and 106 h at 100 and 20 °C, respectively. The data are shown by the curve marked heating scan in Fig. 6. The conductivity measurement was initiated at 0 °C, data were collected at 20 °C intervals after equilibrating the specimen for 30 min at the measurement temperature, and finally the measurement was terminated at 100 °C. The temperature dependence data suggest an absence of crystalline PEO with conductivity values ranging from $10^{-5.4}$ to $10^{-3.2}$ S cm^{-1} between 0 and 100 °C. After the specimen was held overnight at 100 °C, the conductivity at the temperature decreased from $10^{-3.2}$ to $10^{-3.35}$ S cm^{-1}. During the cooling scan to 20 °C, the conductivities remained lower than those obtained from the heating scan. The difference between the heating and cooling scan conductivity values widened as the temperature was lowered. At 20 °C, the specimen was allowed to equilibrate overnight. During a span of 16 h, conductivity increased from $10^{-5.25}$ to $10^{-4.55}$ S cm^{-1}. With further reduction in temperature, as expected, the conductivity decreased and approached a value of $10^{-8.6}$ S cm^{-1} at −40 °C.

The degree of conductivity enhancement during isothermal stabilization at 20 °C is almost twice as large as the specimen containing 10% MgO (Fig. 5). The enhancement is related to the weight fraction of the ceramic phase MgO. In this specimen, there are more MgO colloids surrounded by electrified surfaces which rearrange during the isothermal hold and contribute to the conductivity enhancement.

3.3.1.3. PEO:$LiBF_4$ (8:1)–MgO (30 wt.%) electrolyte. The conductivity data of a PEO:$LiBF_4$ (8:1)–MgO (30 wt.%) specimen heat treated under three different times and temperatures are shown in Fig. 7. In general, the conductivity decreased with increasing heat treatment temperature and time. A major change in the slope of conductivity plots at 60 °C for the three sets of data during cooling signifies crystallization of the polymer phase. This characteristic was absent in the 10 and 20% MgO material,

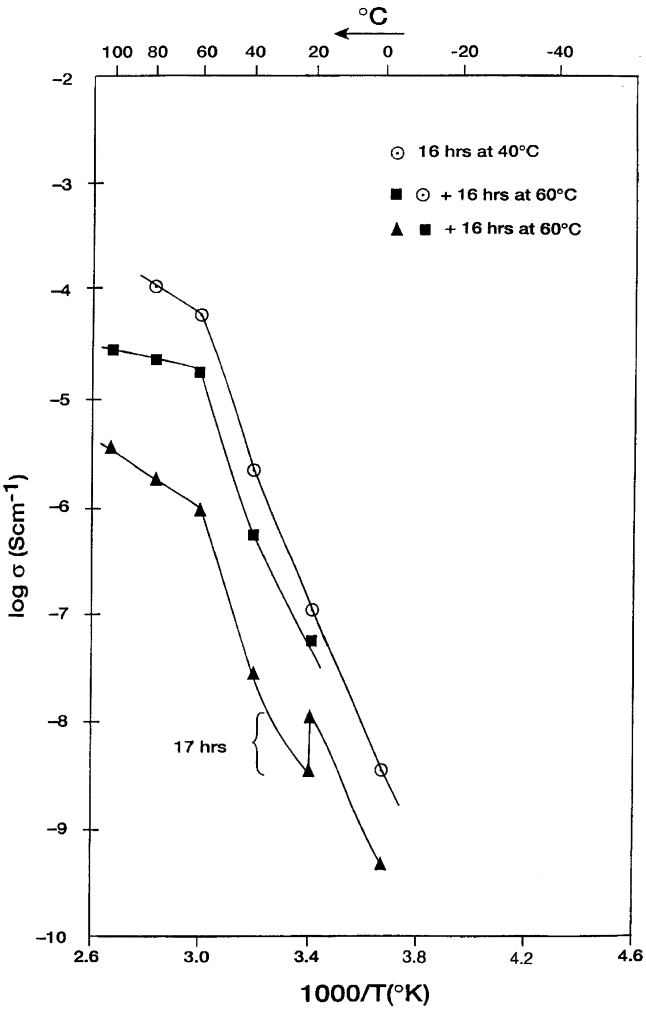

Fig. 7. Temperature dependence of conductivity of PEO:$LiBF_4$ (8:1)–MgO (30 wt.%) electrolyte subjected to three heat treatments.

Figs. 5 and 6. Furthermore, a conductivity relaxation at 20 °C is also shown for the specimen heat treated at 40 and 60 °C for 64 and 16 h, respectively. The conductivity of the specimen subjected to the heat treatment was enhanced by isothermal stabilization of the specimen for 17 h; however, the conductivity remained lower than prior heat treatments and other specimens.

The densities of the PEO:$LiBF_4$ complex and MgO are 1.20 and 3.58 gm cm^{-3}, respectively. If MgO particles are assumed to be uniformly dispersed in the polymer matrix, the estimated lateral spacings for 10, 20, and 30 wt.% MgO specimens are 37, 28, and 24 nm, respectively (Appendix A). The MgO particles in the polymer matrix form a double layer as described in the preceding section. As the concentration of the MgO particles is increased, the lateral spacing between the MgO particles decreases and the protective double layer around each MgO particle breaks down. The breakdown of the double layer is followed by a segregation and formation of heterogeneous MgO nuclei with radii greater than the critical radius on which the polymer phase may crystallize and grow. These interparticle spacings also provide an estimate of the double layer thickness between 5 and 10 nm for these specimens around ambient temperature. It is apparent that these interparticle spacings and double layer thicknesses will depend upon the polymer system, ceramic particle size and shape, and temperature.

3.3.2. *PEO:$LiBF_4$–TiO_2 system*

This system was also investigated and reported earlier [10,11]. The average particle size of TiO_2 was 21 nm and the specimens were made by the solution casting process.

3.3.2.1. *PEO:$LiBF_4$ (8:1)–TiO_2 (20 wt.%) electrolyte.*

Fig. 8 shows the temperature dependence of conductivity of the PEO:$LiBF_4$ (8:1)–TiO_2 (20 wt.%) electrolyte subjected to a wide range of heat treatments. It should be noted that the effect of heat treatment in the 60–100 °C range is pronounced. For example, the room temperature conductivity increases by almost three orders of magnitude between two extremes of the heat treatment schedule. Furthermore, the conductivity enhancement is also associated with reduced activation energy for lithium transport. It is believed that the thermal energy associated with these heat treatments facilitate long range diffusion of nanosize TiO_2 and formation of a double layer around it. The distribution of TiO_2 nanospheres in the PEO matrix also prevents its crystallization. The thermal history dependent conductivity and structural evolution has also been reported with details in an earlier publication [12].

3.3.2.2. *PEO:$LiBF_4$ (8:1)–TiO_2 (30 wt.%) electrolyte.*

Fig. 9 depicts the conductivity evolution of PEO:$LiBF_4$ (8:1)–TiO_2 (30%) as a function of heat treatment. As-prepared film exhibits conductivity typical of PEO-based electrolytes. A heat treatment at 87 °C for 21 h raises ambient temperature conductivity by four orders of magnitude. However, unlike the PEO:$LiBF_4$ (8:1)–TiO_2 (20%) specimens shown in Fig. 8, further heat treatments reduce low-temperature conductivity. This is attributed to migration and coalescence of TiO_2 colloids.

The conductivity data of Figs. 8 and 9 convincingly demonstrate the importance of heat treatment. Prior investigations on polymer–ceramic composite electrolytes have

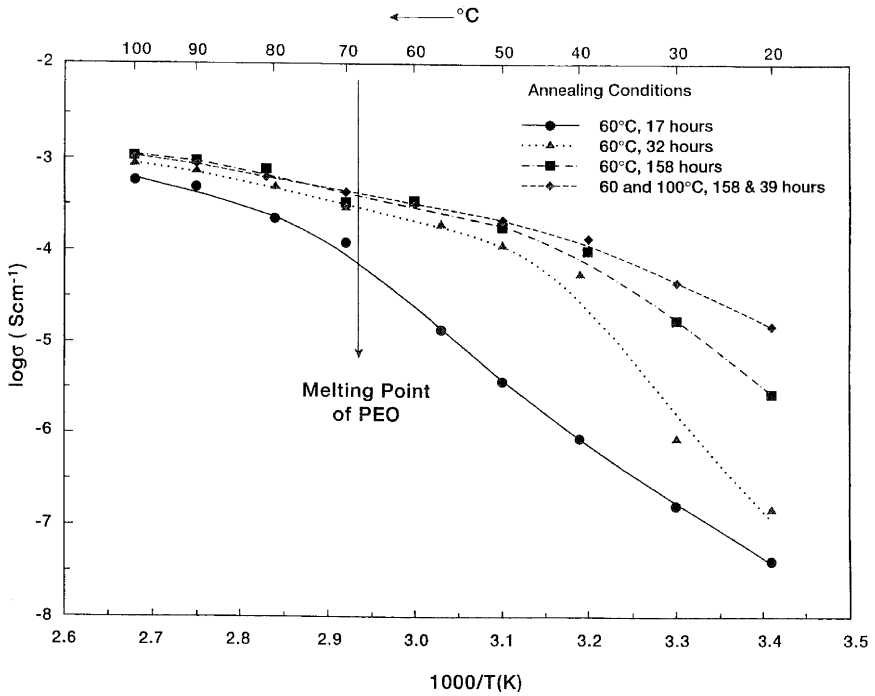

Fig. 8. log σ vs. 1000/T (K) of PEO:$LiBF_4$–TiO_2 (20 wt.%) electrolyte annealed under various conditions.

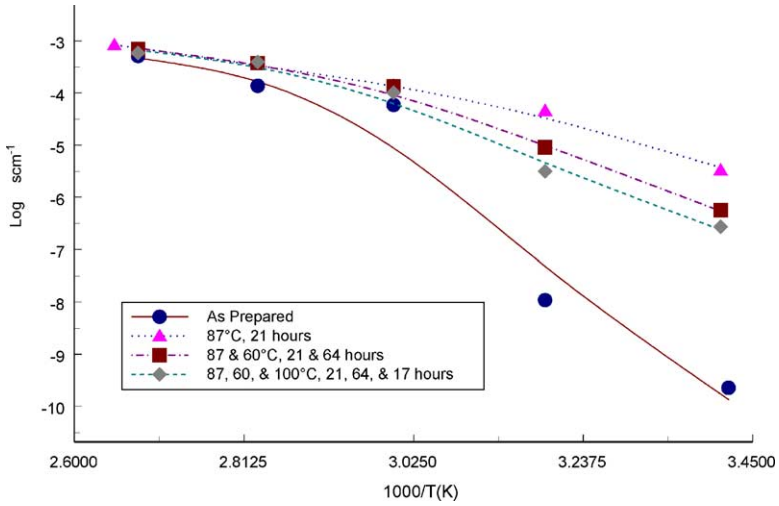

Fig. 9. $\log\sigma$ vs. $1000/T$ (K) of PEO:$LiBF_4$–TiO_2 (30 wt.%) electrolyte annealed under various conditions.

paid little attention to this processing variable and perhaps this may account for the broad range and sometimes even inconsistent results.

The conductivity data presented in Figs. 8 and 9 also illustrates the degree of conductivity enhancements achievable at lower temperatures; i.e., below the melting point of PEO. At higher temperatures, the conductivity enhancement is not as pronounced as at lower temperatures. This also suggests that the transport mechanism around and above the melting temperature is liquid-like and the contribution of the TiO_2 nanoparticle and associated double layer to conductivity is minimal.

It is interesting to compare and contrast the conductivity data of PEO:$LiBF_4$–MgO (30 wt.%), Fig. 7, and PEO:$LiBF_4$–TiO_2 (30 wt.%) TiO_2, Fig. 9. In the case of the MgO-containing electrolyte, the drop in conductivity with heat treatment is precipitous, whereas it is slow and gradual for the TiO_2-containing specimen. The specimen with TiO_2 contains a lesser number of colloids than the MgO-containing specimen because the density and particle size of TiO_2 (4.26 gm cm^{-3} and 21 nm) are greater than the density and particle size of MgO (3.58 gm cm^{-3} and 15 nm). Thus, the interparticle spacing (28 nm versus 24 nm) increased and interaction among them is reduced in the case of the TiO_2 specimen. This is reflected by a decreased sensitivity of conductivity variation with heat treatment parameters.

3.3.3. *PEO:$LiBF_4$–ZrO_2 system*

This system has also been investigated and complete experimental data were presented in an earlier publication [11]. The particle size of ZrO_2 powder was 30 nm.

A PEO:$LiBF_4$–ZrO_2 (30 wt.%) specimen with an [O]:[Li] ratio of 12.64:1 was subjected to two different durations, 18 and 36 h, of heat treatment at 100 °C prior to the conductivity measurement. The measurement was initiated at 100 °C and terminated at 0 °C. At each temperature the specimen was allowed to equilibrate for 15 min. The conductivity data corresponding to the two different heat treatment durations are shown in Fig. 10. A conductivity crossover takes place around the T_m, which could be attributed to melting and crystallization of PEO above and below the T_m, respectively. Above T_m, the liquid medium facilitates transport, whereas below T_m the crystalline PEO hinders transport of lithium.

Also shown in Fig. 10 are two additional conductivity points at 20 °C corresponding to two unique thermal histories. The point with the highest conductivity value ($\log\sigma = -4.68$) was obtained from the specimen which was heated to 148 °C and held at the temperature for 10 min and then cooled down to 20 °C rapidly where it was held for 45 h before conductivity was measured. After obtaining this conductivity value, the specimen was heat treated at 100 °C for 36 h. Subsequently, it was brought down to and held at room

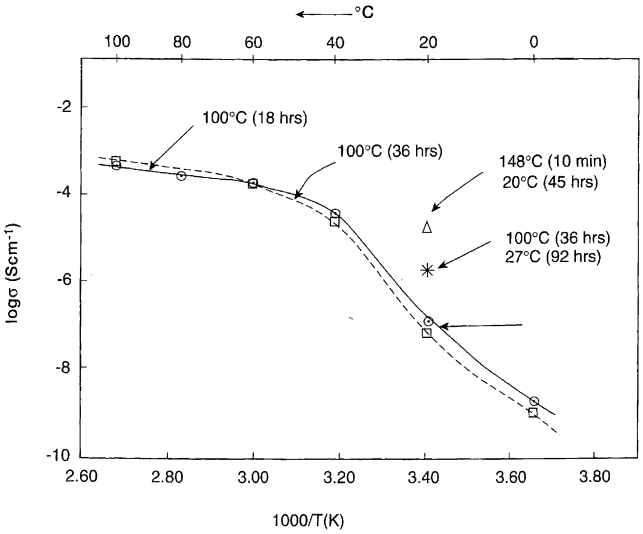

Fig. 10. PEO:$LiBF_4$–ZrO_2 (30 wt.%) specimen with [O]:[Li] ratio of 12.64:1.

temperature for 92 h. Its conductivity was then measured at 20 °C (also shown in Fig. 10) with a $\log \sigma$ value of approximately −5.85. It should be noted that the conductivity at 20 °C ranges from $10^{-7.12}$ to $10^{-4.68}$ S cm^{-1}. The greater than two orders of magnitude difference between the lowest and highest conductivities at 20 °C is attributed to the thermal history effects, polymer chain–ceramic particle interaction, and also crystallization ⇔ melting transition of the PEO.

3.3.4. PEO:LiX–$BaTiO_3$ systems

A number of composite formulations from the PEO:LiX–$BaTiO_3$/Al_2O_3 systems have also been investigated in our laboratory and the experimental data have been published elsewhere [13–15]. $BaTiO_3$ is a ferroelectric ceramic and it was anticipated that this ceramic phase may lead to enhanced conductivity because it provides a localized source of electric field. However, it was determined that $BaTiO_3$ also acts like other ceramic components [13]. Al_2O_3 is a readily available and inexpensive ceramic material and its performance in polymer–ceramic composite electrolytes is similar to other ceramics [15].

3.3.5. Effect of ceramic particle size

Temperature dependence of conductivity of the PEO:$LiBF_4$ complex and PEO:$LiBF_4$ (8:1)–MgO (10 wt.%) materials containing micro- and nanosize MgO are shown in Fig. 11. All these specimens were cycled between 20 and 100 °C three times while holding the specimens for a total cumulative time of 1 h at 100 °C and 40 h at 20 °C. The thermalization process was determined to be adequate to stabilize and optimize conductivity values. Furthermore, at each temperature the specimen was held for 30 min before an impedance measurement was conducted.

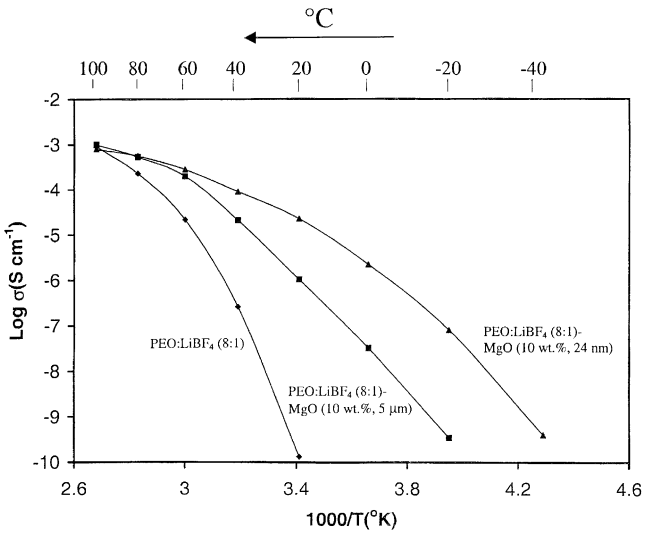

Fig. 11. Temperature dependence of the conductivity of PEO:$LiBF_4$ (8:1)–MgO (10 wt.%).

The lowest conductivity values are associated with the PEO:$LiBF_4$ (8:1) complex. Near the melting point of PEO, 68 °C, a precipitous drop in conductivity begins, and at around ambient temperature the conductivity drops to 10^{-9} S cm^{-1}. The specimen containing microsize (∼5 μm) MgO exhibits much improved conductivity as compared to the PEO:$LiBF_4$ complex. Around ambient temperature, the conductivity is improved by approximately three orders of magnitude by the incorporation of microsize MgO in the polymer complex. This conductivity enhancement is attributed to a large reduction in the crystalline component of the polymer phase. There is a possibility of a residual structural order resembling crystallinity in this composite material as the entire conductivity curve appears to be composed of two linear segments intersecting at the melting temperature of PEO. The highest conductivity values are associated with the specimen containing nanosize MgO. The conductivity of this specimen is about four orders of magnitude higher than the PEO:$LiBF_4$ complex around the ambient temperature. Furthermore, the temperature dependence of conductivity diminished as the MgO particle was reduced from micro- to nanosize. At 100 °C, all three specimens possess similar conductivity values, whereas the curves diverge as the temperature is lowered to −40 °C. It should also be noted that major benefits in conductivity enhancement are realized at lower temperatures by the incorporation of MgO. It has also been reported [8] that increasing the concentration of nanosize MgO from 10 to 20 wt.% makes an insignificant difference in conductivity values.

3.3.6. Prior work on the transport mechanism in composites

The theory of ionic conduction in solid composites was developed by Maier [16–18] in the last two decades. The theory highlights the importance of space charge region or phase boundaries. The boundaries provide a three-dimensional percolation pathway for the transport of charge carriers. Although the theory was developed for interfaces generated by solid–solid interaction, it is plausible that the theory may be extended to cover frozen interfaces created by under- or super-cooling of solid–liquid interfaces. However, no attempt has been made to apply the theoretical development to the colloidal/composite electrolytes described in this paper. The similarity in the temperature dependence of the conductivity of composite type of materials (LiI–Al_2O_3, frozen colloidal electrolytes, polymer–ceramic composites) suggest that the underlying transport mechanism and the structure of the three-dimensional conduction path may be similar.

3.4. Peculiarities (chemical interaction, thermal history dependence, and hysteresis effect)

In the preceding section it has been shown that the conductivity, σ, of composite electrolytes is dependent upon

heat treatment parameters such as temperature (50–150 °C) and time (soak time and heating and cooling rates). This phenomenon was described as thermal history effects and conductivity relaxation in our previous publications [11,13]. These effects are pronounced and peculiar in the sense that they were not recognized or addressed in any significant depth in spite of world-wide interest in polymer electrolytes for over two decades. This section will present studies conducted primarily in our laboratory to delineate these peculiarities.

3.4.1. Polymer chain–ceramic particle interaction

In spite of widely different physical characteristics, including density and dielectric constant, ceramic additives exhibit identical effects with similar particle size. A variation in particle size of a given ceramic material markedly affects the conductivity and thus it is believed to be a dominant parameter. Reducing the particle size from the micro- to nano-range increases low-temperature conductivities and decreases their temperature dependence. The enhancements are pronounced and associated with lower activation energies for the lithium transport.

The average length and mass of a PEO chain are 20 μm and 3×10^{-18} g, respectively. These length and mass values must now be compared with the particle size and mass of the ceramic dopants, for example MgO, to develop an insight into possible interactions. Schematically, the proximity and interaction of a polymer chain and a nano-size MgO particle (0.02 μm) are shown in Fig. 12. A constant segmental chain motion at ambient temperature, approximately 70 °C above the glass transition temperature, is expected to cause displacement and distribution of MgO particles. Furthermore, the process can be facilitated by thermal treatments and cycling. The displacement and distribution of MgO particles continues until the polymer chain dipole and MgO dipole interaction takes place. The interaction leads to latching of the polymer chain and MgO particle and thus stabilization of the structure. When experimentally monitored, this phenomenon is reflected by an increase in conductivity during isothermal stabilization at low temperatures.

The degree of polymer chain and ceramic particle interaction can be enhanced by a lighter, greater in number, and higher weight or volume percent of MgO. For example, if the weight percent of MgO is maintained constant and the particle size is reduced from 5 μm to 20 nm, over 15 million additional polymer–ceramic interaction sites are created and conductivity enhancements occur. A reduction of particle size from 5 μm to 20 nm reduces the mass of a particle by seven orders of magnitude. These lighter MgO particles become far more receptive to the segmental chain motion of the polymer, leading to improved polymer chain and MgO particle interaction. Such an interaction is reflected by an enhanced and time dependent conductivity.

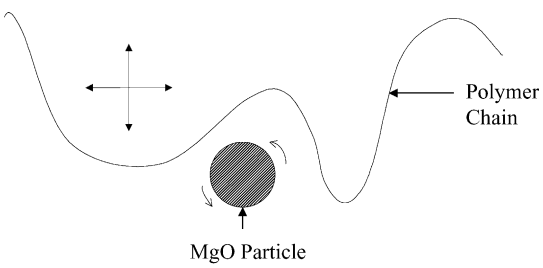

Fig. 12. Schematic representation of a polymer chain segment and MgO particle interaction.

The interaction between polymer and ceramic components is also reflected by the appearance of new absorption bands as determined by IR absorption spectroscopy. Absorption bands in the range of 460–530 cm^{-1} develop as a result of MgO addition in the PEO:$LiBF_4$ complex [14]. These bands also shifted to higher frequencies by approximately 21 cm^{-1} after mechanical stretching.

3.4.2. Heating and cooling rate dependent conductivity

A PEO:$LiBF_4$ (8:1)–TiO_2 (20 wt.%) specimen in blocking electrode configuration (stainless steel as blocking electrodes) was heated to 150 °C, held at this temperature for 30 min, and then rapidly cooled to 0 °C. The conductivity of this specimen was measured as a function of temperature and time while the temperature was raised from 0 to 150 °C. The experimental data are shown in Fig. 13. At each temperature there are two data points, an arrow, and a number of hours. The data points represent the range of conductivity values, the arrow pointing upward indicates conductivity enhancement, and the number of hours is the time interval between the two measured values of conductivity. For example, at 0 °C, after the specimen was cooled from 150 °C, the $\log \sigma$ was −9.85. The $\log \sigma$ increased to −9.37 after it was held at the temperature for 114 h. This type of conductivity enhancement appears at all temperatures; however, the degree of enhancement, as measured by the absolute difference between the two data points and normalized for the hold time, diminished as the temperature was raised from 0 to 150 °C.

The specimen whose thermal history and conductivity data are shown in Fig. 13 was equilibrated for 30 min after it reached 150 °C, and then cooled down gradually and slowly to 100, 80, 60, 40, 20, and 0 °C for conductivity measurement. The conductivity values and hold time at each of the temperatures are shown in Fig. 14. In general, the conductivity decreased as the hold time increased at the given temperature. The conductivity variations as a function of hold time at all temperatures above 20 °C were small but measurable and significant. However, the decline in conductivity at 20 °C is pronounced. The conductivity decreased more than an order of magnitude in the first 2–3 h, and comparatively subsequent reduction was small.

An explanation needs to be provided for the enhancement of conductivity with hold time of the specimen in Fig. 13. The heat treatment at 150 °C and rapid cooling to 0 °C was conducted to ensure the formation of amorphous PEO in the specimen, yet the conductivity was very low. But the con-

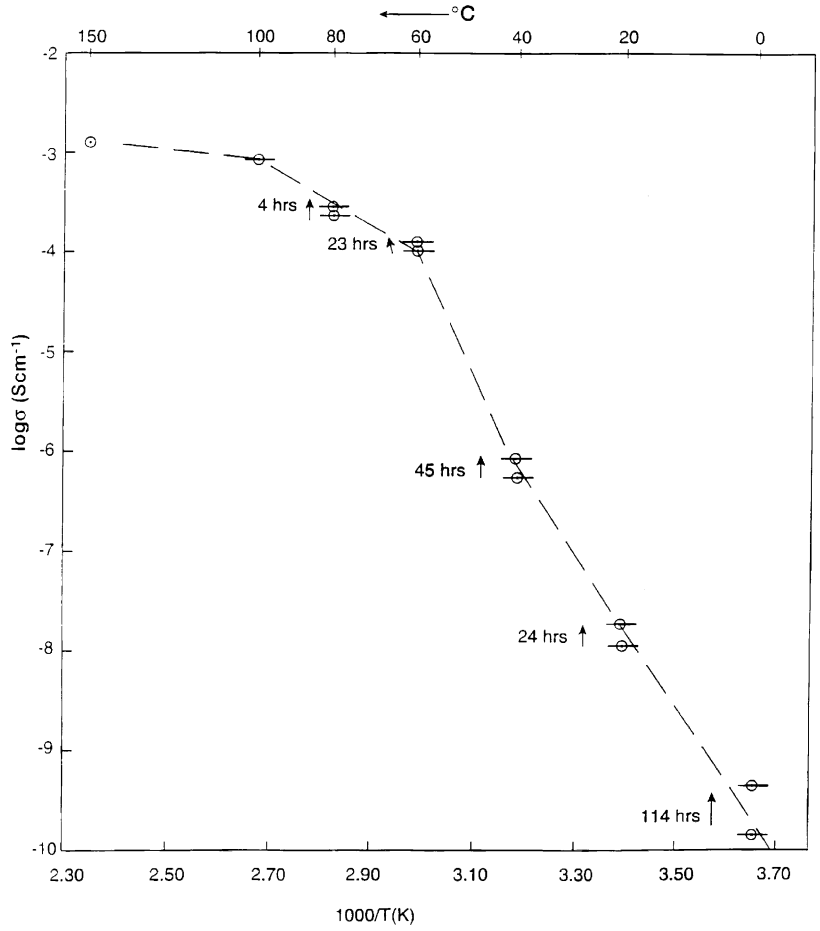

Fig. 13. Conductivity of PEO:$LiBF_4$–TiO_2 (20 wt.%) composite electrolyte during heat-up. The specimen was heat treated at 150 °C for 30 min and then quenched to 0 °C before the conductivity measurement.

ductivity increased with the hold time at all temperatures. This was originally explained on the basis of dipole–dipole interaction [12]. The molecular structure of the PEO:$LiBF_4$ complex and nanosize crystallites of TiO_2 possess permanent dipole moments. These dipoles are electroactive and are building blocks of the composite electrolyte. At high temperatures (≃150 °C), the thermal energy is high enough to disrupt dipole–dipole interaction. The nanosize TiO_2 particles are under constant motion. As the specimen is cooled down to 0 °C, the random positions of TiO_2 particle are frozen. The dipole–dipole interaction begins and formation of a double layer such as shown in Fig. 1 is initiated. A small scale displacement of TiO_2 particles is also envisioned to accommodate the dipole–dipole interaction.

The dipole–dipole interaction is dependent upon the dielectric constant gradient between the polymer and ceramic components. The dielectric constant, κ, is related to the polarization, P, and local electric field, E_L, through Eq. (1):

$$\kappa = 1 + \frac{P}{\varepsilon_0 E_L} \tag{1}$$

where ε_0 = permittivity of free space. Furthermore, it can be demonstrated [19] that the second term of Eq. (1) is related to the number of dipoles, n:

$$\frac{P}{\varepsilon_0 E_L} = \frac{nz^2e^2b^2}{4kT} \tag{2}$$

Substitution of Eq. (2) in Eq. (1) leads to an expression, Eq. (3), relating κ and n:

$$\kappa = 1 + \frac{nz^2e^2b^2}{4kT} \tag{3}$$

From Eq. (3) it is apparent that the κ increases linearly with decreasing temperature and slope, which is determined by the number of dipoles, n, as other parameters are constant. In a composite electrolyte, the polymer phase is associated with a lower dielectric constant as compared to the ceramic phase. Thus, a dielectric constant gradient ($\Delta\kappa$) exists at the nano-structure level. This gradient is proposed to be the driving force for the polymer–ceramic interaction and formation of a double layer. The interaction is favorable at lower temperatures (≃20 °C) and may be diminished or even eliminated at higher temperatures (≃100 °C). As discussed earlier, these double layers enhance the transport of conducting species in the composite specimen.

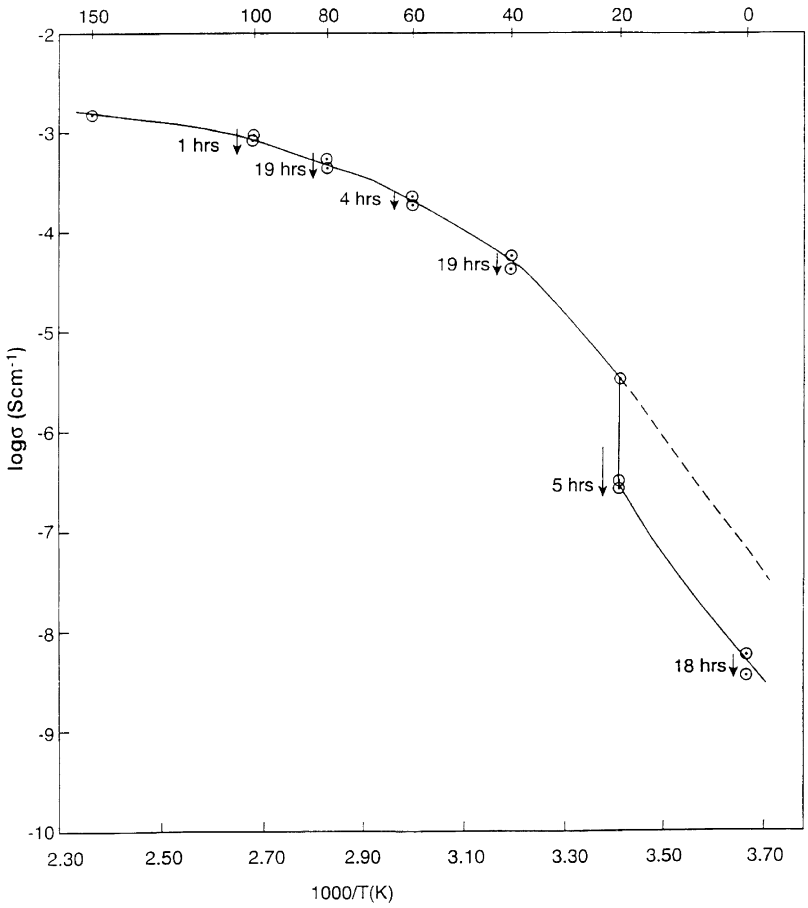

Fig. 14. Conductivity of PEO:$LiBF_4$–TiO_2 (20 wt.%) composite electrolyte heat treated at 150 °C for 30 min. The conductivity was measured while the specimen was slowly cooled from 150 °C and stabilized at the temperature of measurement.

It is evident that ceramic particles not only render the PEO matrix to exist in the amorphous state, but they also interact with its elementary units. The belief that the enhancement of conductivity in polymer–ceramic composite electrolytes is related to the retention of the amorphous structure is not entirely correct. The polymer chain interaction leading to the formation of the double layer also contributes to the conductivity enhancement and the magnitude of the enhancement is estimated to be over an order of magnitude.

A rapid drop of conductivity at 20 °C as shown in Fig. 14 signifies crystallization of the PEO. The conductivity decreased more than an order of magnitude in the first 2–3 h. A small drop in conductivity at other temperatures, Fig. 14, is attributed to the randomization of TiO_2 colloids and a breakdown of double layers driven by the thermal energy.

3.4.3. Physical aging effects on conductivity

The term physical aging implies a relaxation of the amorphous structure from a nonequilibrium to an equilibrium state with the passage of time. The term also distinguishes amorphous state relaxation from other time-dependent structural transitions such as recrystallization and chemical degradation. The physical aging occurs in the vicinity of the glass transition temperature, T_g, and thermodynamic parameters such as volume, enthalpy, and entropy decrease as a result of physical aging. This section presents a study conducted on the physical aging of a PEO:$LiClO_4$ (8:1)–Al_2O_3 (20 wt.%) composite electrolyte specimen. The details of this investigation have been published earlier [20].

3.4.3.1. Physical aging and conductivity relaxation. An amorphous polymer undergoes a transformation from a nonequilibrium to an equilibrium state at a unique rate determined by the thermodynamic parameters. Such a system is under internal stress, and the transformation occurs to relieve the stress. The transformation occurs by a relative displacement of structural elements of the composite electrolyte. It relieves the internal stresses at points known as relaxation sites. The kinetics of the relaxation largely depends upon the characteristics of the relaxation site. A composite electrolyte may also possess more than one kind of relaxation site. Associated with the various relaxation sites are characteristic relaxation times. The result of this transformation is a change in the physical properties (in this case, the conductivity) of the material, which occurs through a double layer rearrangement.

The conductivity relaxation of composite electrolytes at a given temperature may be expressed by Eq. (4):

$$\sigma'(t) = \sigma(\infty) \pm \sum_{i=0}^{n} \sigma_i \, e^{-\nu_i t} \quad (4)$$

where $\sigma'(t)$ is the theoretical conductivity at time t; $\sigma(\infty)$ the equilibrium conductivity; σ_i the relaxation amplitude; ν_i the relaxation frequency ($1/\tau_i$); τ_i the relaxation time

Eq. (4) introduces the most difficult aspect of physical aging: the complexity and nonlinearity resulting from the collective effect of a large number of relaxation sites. Furthermore, the physical aging exhibits a memory effect; relaxation from a given state not only depends upon that state but also on how that state was reached. For example, the conductivity of a polymer–ceramic composite that has been melt cast will depend upon its temperature, mechanical deformation history during hot pressing, and post-processing thermal history before the composite is put into service or characterized.

To circumvent the analytical complexity of physical aging, it was proposed to assume that there is only one kind of relaxation mechanism during the early stages of physical aging [11]. If such an assumption is carried out, Eq. (4) is reduced to

$$\sigma(t) = \sigma'(t) - \sigma(\infty) = \sigma_0 \, e^{-\nu_0 t} \quad (5)$$

where $\sigma(t)$ is the experimentally measured conductivity at time, t. The validity of the assumption will be assessed by the experimental data. A plot of $\ln \sigma(t)$ versus t should therefore yield a straight line from which the relaxation time, τ_0, can be calculated.

After a PEO:$LiClO_4$ (8:1)–Al_2O_3 (20 wt.%) composite electrolyte specimen was thermally cycled five times between 20 and 100 °C to ensure the existence of only an amorphous phase, the conductivity as a function of time was measured. The conductivity relaxation data at 20, 30, 40, 50, 60, and 70 °C of a specimen of the composition are shown in Fig. 15. As shown in Fig. 15, the conductivity relaxation was monitored only up to 24 h, which may be considered an early stage of the physical aging. The aging may continue for months before the equilibrium state is reached. A regression analysis of the data exhibits a linear relationship at each of the temperatures, giving credence to the assumption of a single relaxation mechanism. The correlation coefficients, r, obtained from the regression analysis at each temperature are also shown in Fig. 15. The highest value of the correlation coefficient, 0.9976, noted at 40 °C, decreases if the temperature is either lowered or increased. The relaxation times, τ_0, of 93, 36.6, 33.4, 31.45, 37, and 88.5 h correspond to aging temperatures of 20, 30, 40, 50, 60, and 70 °C, respectively, as obtained from the data.

A plot of the relaxation time, τ_0, as a function of temperature is shown in Fig. 16. The U-shaped temperature dependence of the relaxation time presents some interesting insights into the structure, processing, and performance during use of these composite electrolytes. The data show that the structural stabilization is the fastest at 50 °C (lowest τ_0), and thus this temperature should be considered as the optimal annealing temperature of the composite electrolyte. As the temperature is lowered, the relaxation time increases and becomes inordinately high at 0 °C. An increase in temperature above 50 °C increases the relaxation time and may be associated with a liquid-like behavior. The uncertainty in the measurement of the relaxation time as expressed by the correlation coefficient, r, also increases as the temperature deviates from 50 °C. The processing parameters of these composite electrolytes are expected to have considerable influence on their properties. For example, a rapid cooling from a temperature above 70 to 20 °C will lead to an unrelaxed (destabilized) structure with low conductivity. Storage of the specimen at 20 °C will lead to an increase in conductivity with time until it reaches an equilibrium value. Consistent with the aforementioned memory effect, a more complex structural evolution may be expected when the specimen is brought from −40 to 20 °C. In this case, the thermal history before the specimen was brought to −40 °C would also influence conductivity evolution at 20 °C.

In view of the aforementioned attributes associated with U-shaped temperature dependent relaxation time, the conductivity of the specimen was measured at 20 °C employing two distinct thermal histories. In the first thermal history (t_1), the specimen was cooled down from 20 to 0 °C where it was stabilized for 2 h and subsequently heated to 20 °C when time dependent conductivity was measured. In the second thermal history (t_2), the specimen was heated from 20 to 40 °C, held at 40 °C for 2 h, and subsequently cooled down to 20 °C for the measurement of time dependent conductivity. The time dependent conductivities of the specimen with thermal histories t_1 and t_2 are presented in Fig. 17. The conductivity evolution associated with the two thermal histories is nonlinear and parallel but significantly different. The t_1 thermal history gives rise to about 20% higher conductivity.

The higher conductivity associated with the thermal history t_1 may be attributed to two factors: structural densification and dipole–dipole interaction leading to double layer formation. The stabilization of the specimen at 0 °C for 2 h leads to a densification of the structure. The dielectric constants of solids increase as the temperature is decreased, which may enhance the [O–CH_2–CH_2] dipole and Al_2O_3 dipole interaction. Both of these factors are proposed to contribute to the higher initial conductivity of the specimen associated with the thermal history t_1. Interestingly, the conductivity continues to increase with time nonlinearly at 20 °C, which is attributed to further densification, dipolar interaction, and double layer formation of the structure. The relaxation curves characteristic of the two thermal histories are expected to merge at longer times.

A schematic illustration of the composite electrolyte structure is shown in Fig. 18, illustrating segments of the PEO chain forming helices in which lithium ions reside. The oxygens of the PEO are polarized to form dipoles whose nega-

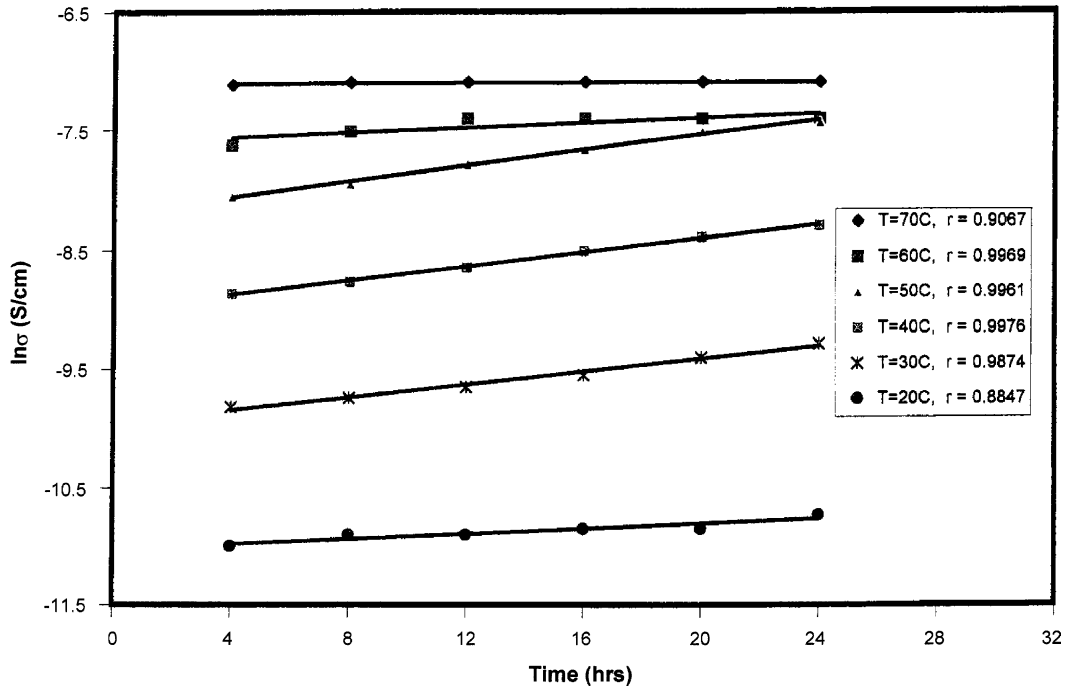

Fig. 15. Time dependence of conductivity of the PEO:$LiClO_4$ (8:1)–Al_2O_3 (20 wt.%, 24 nm) at 20, 30, 40, 50, 60, and 70 °C.

tive sides are coordinated to lithium ions. The geometry and size considerations require that the anion ClO_4^- and Al_2O_3 particles reside outside the PEO helices. The concentration of ClO_4^- outnumbers Al_2O_3 particles by approximately five orders of magnitude. Fig. 18 illustrates the structure in the vicinity of an Al_2O_3 particle. The structural arrangement maintains local electrical neutrality and is consistent with the double layer structure illustrated in Fig. 3(a) and (b). The experimental conductivity data and the structure illustrated in Fig. 18 suggest that physical aging reduces the size of the coordinating sphere around the lithium ion and enhances the double layer structure. Furthermore, the size of the coordinating sphere is dependent on the temperature and heating or cooling rate in the processing and application temperature range.

The experimental data and discussions presented in this paper are inconsistent with the free volume concept, which suggests that the mobility of particles should decrease with increasing degree of packing, initially slowly but later at an increasing rate. The data presented in this section clearly

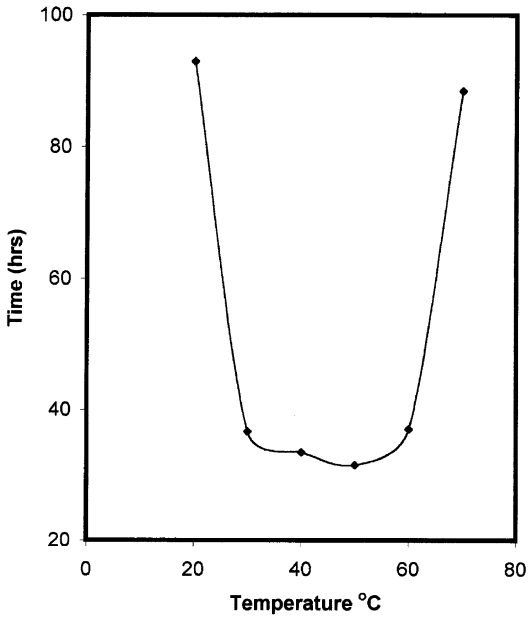

Fig. 16. The structural relaxation time, τ_0, as a function of temperature of the PEO:$LiClO_4$ (8:1)–Al_2O_3 (20 wt.%, 24 nm) composite electrolyte.

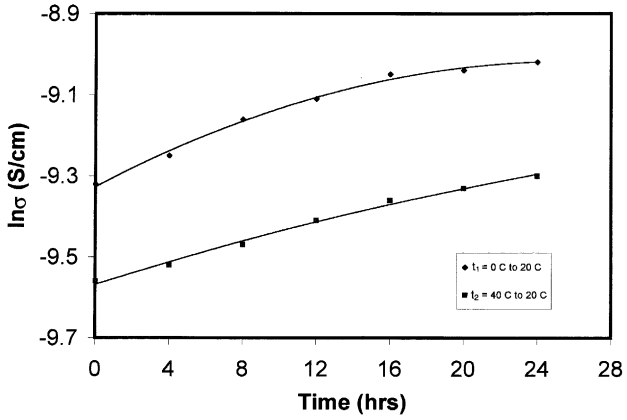

Fig. 17. Time dependence of conductivity at 20 °C of the PEO:$LiClO_4$ (8:1)–Al_2O_3 (20 wt.%, 24 nm) specimen with two thermal histories t_1 and t_2.

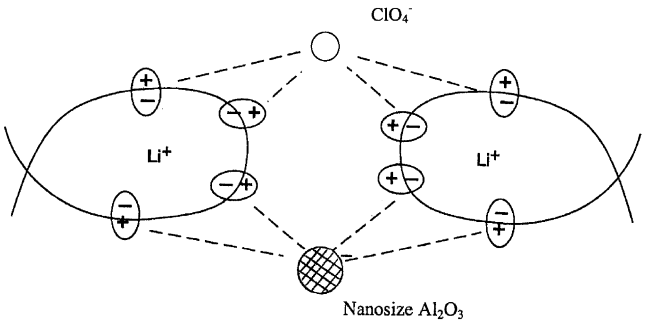

Fig. 18. Schematic structure of PEO:$LiClO_4$ (8:1)–Al_2O_3 (20 wt.%, 24 nm) composite electrolyte.

suggest that increased packing resulting from the physical aging enhances ionic mobility. Struik [21] also arrived at a similar conclusion while analyzing physical aging and the free volume concept.

Conductivity of an aged specimen. The temperature dependence of conductivity of the PEO:$LiClO_4$ (8:1)–Al_2O_3 (20 wt.%, 24 nm) specimen after aging at various temperatures in the −40 to 100 °C range after a period of 6 weeks is shown in Fig. 19. Relatively small temperature dependence is observed in the 20–100 °C temperature range. As the temperature is lowered towards T_g, the temperature dependence is increased. An interaction of polymer structural unit with $LiClO_4$ and nanosize Al_2O_3 produces a noncrystalline polymer matrix structure in which Al_2O_3 particles are uniformly distributed. The interaction between the polymer and Al_2O_3 phases leads to the formation of a double layer which facilitates transport of conducting ions. The noncrystalline structure of the composite specimen provides small temperature dependence in the 20–100 °C temperature range. As the temperature is lowered below 20 °C, the conductivity is associated with a larger temperature dependence.

The conductivity of the PEO:$LiClO_4$ (8:1)–Al_2O_3 (20 wt.%, 24 nm) specimen at 20 °C is about 0.64 m S cm^{-1}, a much higher value compared to conductivity of similar specimens reported in Ref. [9]. It should also be noted that even after extensive aging for 45 days, there was no chemical degradation of the specimen.

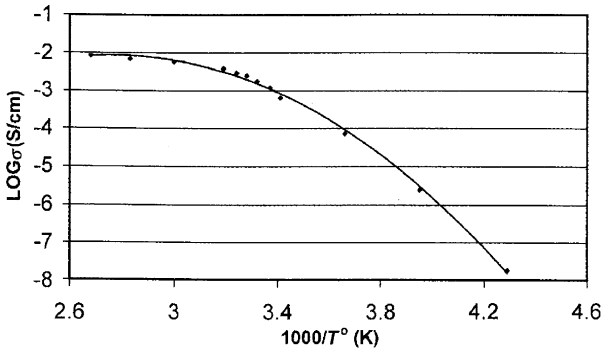

Fig. 19. Temperature dependence of conductivity of PEO:$LiClO_4$ (8:1)–Al_2O_3 (20 wt.%, 24 nm) solid electrolyte.

3.4.4. Electrophoresis in polymer–ceramic composite electrolytes

For a while it was believed that the conductivity enhancements in composite electrolytes originated from dipolar alignments [12,14]. At the time, a relationship between the dipolar alignment and double layer formation was not understood or established. On a macroscopic level, if it can be assumed that the dipoles associated with polymer chains and ceramic particles possess random orientation, then the application of an electric field should orient the dipoles and an enhancement in conductivity should follow. In view of this hypothesis, an electrolyte specimen of PEO:$LiBF_4$ (8:1)–MgO (10 wt.%) composition in the blocking electrode configuration was heated to 100 °C and a dc field of 10 V cm^{-1} was applied across the specimen. Subsequently, the specimen was cooled down to 20 °C and after removal of the dc field, conductivity was measured by the impedance technique.

Fig. 20 shows the temperature dependence of conductivity of the specimen with and without the applied dc field. During a cooling scan, the specimen without an applied dc field

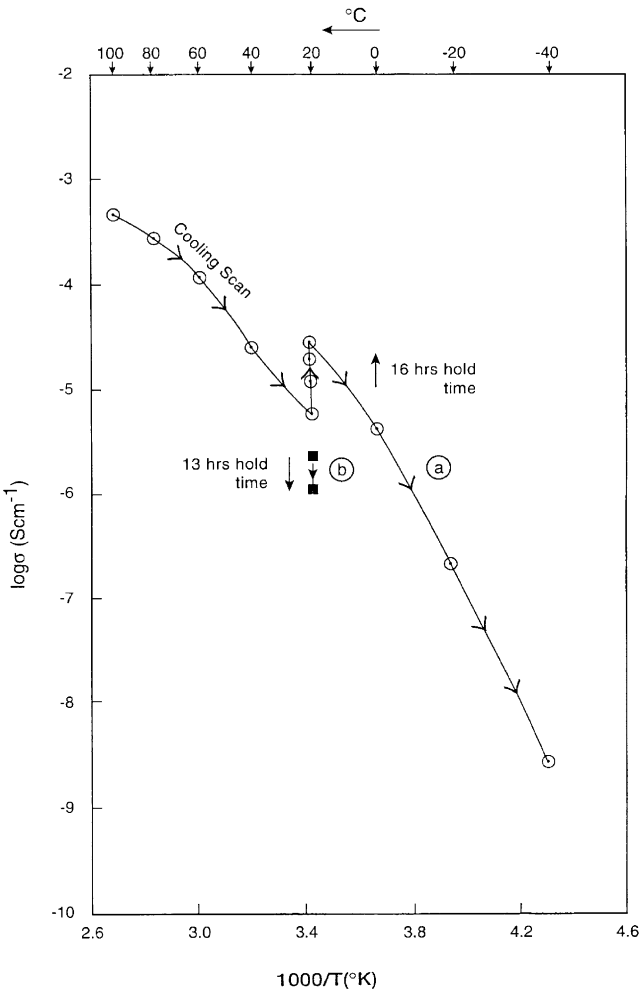

Fig. 20. Conductivity of PEO:$LiBF_4$ (8:1) (10 wt.%) (a) during cooling scan and isothermal stabilization at 20 °C, and (b) dc field-assisted, rapidly quenched specimen isothermally stabilized at 20 °C.

was held at 20 °C for 16 h and the conductivity increased by almost an order of magnitude—a situation similar to other composite electrolyte specimens discussed.

After the specimen was rapidly quenched under the dc field from 100 to 20 °C, the measured conductivity ($\log\sigma = -5.64$) was 33% lower than the value ($\log\sigma = -5.24$) obtained during the standard cooling scan. This observation contradicted the hypothesis. There was an effect of the dc field assisted cooling on conductivity, but it was negative.

The lower conductivity of the dc field-assisted, rapidly quenched specimen is now attributed to migration (electrophoresis), polarization, and coalescence of MgO colloids. The MgO colloids must have piled onto one of the electrodes under the applied dc field. An isothermal hold of the specimen at 20 °C for 13 h further decreased the conductivity, which is also shown in Fig. 20. Most of the specimen was now depleted of MgO colloids after the application of the field. Subsequently, the specimen exhibited characteristics of a typical PEO-based polymer electrolyte; i.e., it crystallized and conductivity dropped.

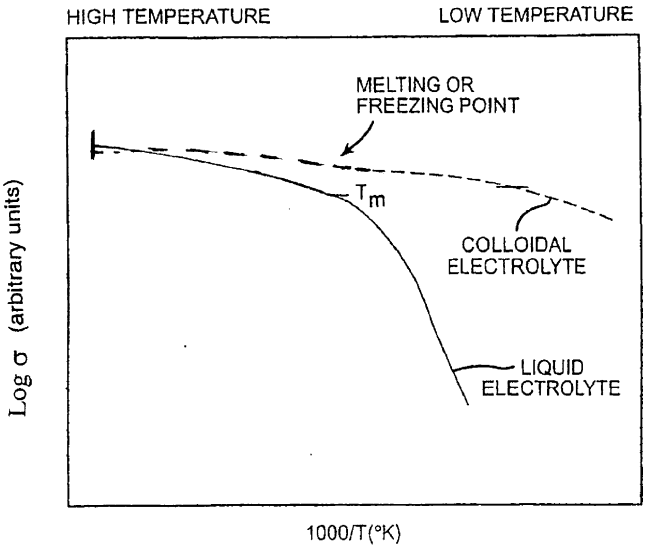

Fig. 21. A schematic presentation of temperature dependence of conductivity of liquids, polymers, and colloidal electrolytes.

4. Possibilities

This paper has covered attributes of emerging colloidal and polymer–ceramic composite electrolytes. These electrolyte systems are lithium ion conductors and the analysis of a broader range of electrolytes reveals that the incorporation of ceramic components in a liquid or polymer matrix leads to conductivity enhancement at lower temperatures. This implies that the temperatures are lower than the freezing temperature of a liquid electrolyte or the melting point of polymer electrolytes.

A collective evaluation of conductivity data and related observations on liquid, polymer, and polymer–ceramic composite electrolytes obtained in our laboratory and elsewhere leads to a general observation. This observation, schematically presented in Fig. 21, can be applied to colloidal and composite electrolytes. At higher temperatures ($>T_m$), liquid and colloidal electrolytes possess comparable conductivity. In some cases, colloidal electrolytes exhibit lower conductivity. As the temperature is lowered to about 10–25 °C below the freezing or melting point, T_m, the colloidal electrolytes begin to display superior conductivity. With further decreases in temperature, the conductivity difference between liquid and colloidal electrolytes widens and about 100 °C below the T_m, the conductivity can differ by orders of magnitude.

The structure of electrolytes below the melting or freezing temperature is expected to have a significant influence on conductivity. In the polymer electrolyte literature, the role of crystalline to amorphous transition is well documented [13,22]. The amorphous structure of polymers is desired, but is not the only parameter affecting the conductivity. The polymer chain–ceramic particle interaction and formation of a double layer are also important. The volume fraction and particle size of the dopants are additional factors for stabilizing amorphous structure below T_m [13]. A similar argument can also be applied while formulating high performance colloidal electrolytes.

A recent review paper [23] discusses polymer–ceramic composite protonic conductors as a membrane material for polymer electrolyte membrane fuel cells (PEMFCs). The composite protonic conductors possess key attributes, such as a superior propensity to retain water, enhanced protonic conductivity, superior thermal and mechanical robustness, and reduced permeability of molecular species. The polymer and ceramic phases chemically interact and provide nanostructures and microstructures beneficial for protonic conductivity, and mechanical and thermal properties.

A number of different processing techniques may be used to prepare film and bulk specimens of colloidal composite electrolytes. The in situ processing technique in which the colloidal phase can be precipitated from a solution or glassy matrix provides for better control over the colloid size, volume fraction, and double layer formation. The blend technique is a convenient processing method in which a liquid polymer, conducting ion salt and nanosize ceramic are mixed in a predetermined proportion, stabilized and contained or pressed into a desired specimen configuration. These two techniques and their variations can provide specimens covering a wide variety of polymers, glasses, and ceramic components.

5. Summary and conclusions

This paper presented and discussed the effects of a colloidal phase on the conductivity of liquid and polymeric electrolytes. The colloidal phase consisted of powders of diverse ceramics such as MgO, TiO_2, ZrO_2, Al_2O_3, and

$BaTiO_3$. These colloids affect low-temperature conductivity. The enhancement in conductivity may be orders of magnitude, depending upon the temperature. The enhancement is also ceramic particle size dependent.

The doping of ceramic components into a polymer matrix leads to the formation and existence of a double layer. Because of excessive thermal energy of ions and electrons at elevated temperatures ($>T_m$), the double layer tends to be diffused and ineffective. However, as the temperature is lowered below the melting or freezing point, the double layer becomes compact and relatively stationary so as to contribute to the motion of conducting ions. The formation and stability of well-defined double layers are believed to be critical for conductivity enhancement in the composite systems. The annealing and physical aging effects originate from the existence and displacement of these double layers surrounding each ceramic particle. This is also believed to be the origin of conductivity hysteresis in the composite electrolytes.

Societal needs and concerns call for concerted measures to deal with issues of human transportation, efficient uses of energy, and global warming. In a broader sense, all these issues are interlinked, and a satisfactory solution will require technological innovations in a number of disciplines, specifically electrochemical industries (fuel cells, batteries, sensors, gas separators, etc.). The composite route for the development of solid state, ionically conducting materials is potentially important for providing quantum evolution to the electrochemical industries. One can design and develop ionic conductors for specific applications by selecting three critical elements: a conducting ion, a transport medium, and a network of double layers in a composite material.

The colloidal composite electrolyte systems covered in this paper are intriguing. They hold a lot of potential for many applications, but are also fairly complicated. It is our hope that this paper may contribute to the justification and inspiration for further work, which will augment our understanding of electrical transport mechanisms, structural details, and long-term performance of these composite systems.

Acknowledgements

The author expresses his gratitude to the Air Force, NASA, and Eagle-Picher, LLC for sponsoring a number of contracts on polymer–ceramic composite electrolytes which generated basic experimental data from which this paper originated.

Appendix A. Computation of interparticle spacing in the PEO:$LiBF_4$–MgO system

Density of PEO : $LiBF_4 = 1.20\,g/cm^3$

Density of MgO $= 3.58 g/cm^3$

Volume of composite electrolyte/g of material

$$= \frac{0.9}{1.2} + \frac{0.1}{3.58} = 0.78\,cm^3$$

$$= 0.78 \times 10^{-6}\,m^3/g \text{ of composite electrolyte}$$

$$\text{Volume of MgO particles} = \tfrac{4}{3}\pi(7.5 \times 10^{-9})^3\,m^3 = 1.77 \times 10^{-24}\,m^3$$

Number of MgO particle/g of composite electrolyte

$$= \frac{2.79 \times 10^{-8}\,m^3}{1.77 \times 10^{-24}\,m^3} = 1.57 \times 10^{16}$$

Number of MgO particles/unit volume of composite electrolyte

$$= \frac{1.57 \times 10^{+16}}{0.78 \times 10^{-6}} = 2.01 \times 10^{22}\,m^{-3} = 2.01 \times 10^{4}\,\mu m^{-3} = 27.2 \text{ particles } \mu m^{-1}$$

The interparticle spacing in PEO:$LiBF_4$–MgO (10 wt.%) = 37.00 nm. Similarly, it can be shown that the interparticle spacings in PEO:$LiBF_4$–MgO (20 wt.%) and PEO:$LiBF_4$–MgO (30 wt.%) materials are 28.00 and 24.00 nm, respectively.

References

[1] B. Kumar, S.J. Rodrigues, Solid State Ion. 167 (1-2) (2004) 91–97.
[2] R.C. Agarwal, R.K. Gupta, J. Mater. Sci. 34 (1999) 1131.
[3] A. Mikrajuddin, G. Shi, K. Okuyama, J. Electrochem. Soc. 147 (8) (2000) 3157–3165.
[4] P. Knauth, J. Electroceram. 5 (2) (2000) 111–125.
[5] B. Kumar, L.G. Scanlon, J. Electroceram. 5 (2) (2000) 127–139.
[6] J.O'M. Bockris, A.K.N. Reddy, Modern Electrochemistry, Plenum/Rosetta edition, 1972, pp. 835–843.
[7] B. Kumar, L.G. Scanlon, J. Power Sources 52 (1994) 261.
[8] B. Kumar, L. Scanlon, R. Marsh, R. Mason, R. Higgins, R. Baldwin, Electrochim. Acta 46 (2001) 1515–1521.
[9] F. Croce, G.B. Appetecchi, L. Persi, B. Scrosati, Nature 394 (1998) 456–458.
[10] B. Kumar, L.G. Scanlon, in: Proceedings of the SAE Aerospace Power Systems Conference, Williamsburg, VA, April 9–11, 1997, pp. 71–82.
[11] B. Kumar, L.G. Scanlon, Solid State Ion. 124 (3) (1999) 239–254.
[12] B. Kumar, L.G. Scanlon, R.J. Spry, J. Power Sources 96 (2001) 337–342.
[13] B. Kumar, S.J. Rodrigues, L.G. Scanlon, J. Electrochem. Soc. 148 (10) (2001) A1191–A1195.
[14] B. Kumar, S.J. Rodrigues, R.J. Spry, Electrochim. Acta 47 (2002) 1275–1281.
[15] M. Nookala, B. Kumar, S.J. Rodrigues, J. Power Sources 111 (2002) 165–172.
[16] J. Maier, Prog. Solid State Chem. 23 (1995) 171.
[17] J. Maier, J. Phys. Chem. Solid 46 (1985) 309.
[18] J. Maier, J. Electrochem. Soc. 134 (1987) 1524.
[19] L.L. Hench, J.K. West, Principles of Electronic Ceramics, Wiley, New York, 1990, pp. 139, 198.
[20] B. Kumar, S. Koka, S.J. Rodrigues, M. Nookala, Solid State Ion. 156 (2003) 163–170.
[21] L.C.E. Struik, Physical Aging in Amorphous Polymers and Other Materials, Elsevier, Amsterdam, 1978.
[22] C. Berthier, W. Gorecki, M. Minier, M.B. Armand, J.M. Chabagno, P. Rigand, Solid State Ion. 11 (1983) 91.
[23] B. Kumar, J.P. Fellner, J. Power Sources 123 (2003) 132–136.